Chapter 5

Cadmium Sulphide: n-Junction and Barrier Partner

5.0 Motivation, Objective, and Abstract

Motivation

Cadmium is a toxic chemical element but still has an exception entity i. e. CdS as a buffer layer in the photovoltaic world. The locus of the n-type CdS buffer layer is photoconductivity, conformal coverage, and optical transmittance. Locus is dependent on deposition technique which always incentivizes the researchers to develop the deposition technique and optimize the n-CdS buffer layer for a large area production.

Objective

- To adjudge the deposition technique of the CdS layer as an n-junction partner of the p-CIGS absorber.
- To markdown physical, optical, and electrical features of CdS layer deposited by Thermal Evaporation, Chemical Bath Deposition, and RF-Sputtering techniques.
- To pattern P2 isolation using Laser (Nd:YAG 1064 nm) and Mechanical scribing techniques.

Abstract

CdS (Cadmium Sulphide) has been studied as a buffer layer to form a heterojunctions layer with an absorber layer in photovoltaic applications. Different techniques have accounted for the deposition CdS layer. We had studied the CdS thin film layer by Thermal Evaporation, Chemical Bath Deposition (CBD), and RF-Sputtering techniques. Structural, microstructural,

optical, electrical, and Photoluminescence (Pl) analysis of CdS thin films have been studied. Urbach energy, dark resistivity, and light resistivity have also been estimated. An attempt of P2 patterning using Laser (Nd:YAG 1064 nm) and mechanical was successfully carried out.

5.1 A Protective Buffer: Cadmium Sulphide Layer

Cadmium sulphide (CdS) plays a key role in various solar cell systems such as CdTe, Cu (In, Ga) Se_2, Cu (In, Ga) S, $Cu_2ZnSnSe_4$. A certified power conversion efficiency of 22.8 % has been recorded for thin-film-based Cu (In, Ga) Se_2 solar cell [1]. Cadmium sulphide is extensively used as an n-type semiconducting layer in a multi-layered Cu (In, Ga) Se_2 solar cell. For the p-n junction of the solar cell, CdS as a buffer layer have explicit properties such as (a) high transparency, (b) thickness should not be too thick to avoid absorption, nor too thin to avoid short circuit with absorber layer, (c) highly resistive to reduce electrical losses in solar cells and (d) highly photoconductive to not alter the solar cell spectral response [2]. Many different techniques have been accounted for depositing the CdS layer. Many researchers had deposited CdS using different techniques such as MOCVD [3], closed space sublimation [4], pulsed direct current magnetron [5], combine dip [6], microwave-assisted CBD [7], electrodeposition [8], RF-sputtering [9], pulsed laser deposition [10], spray pyrolysis [11], screen printing [12], and chemical vapour deposition [13]. Among all deposition techniques, Chemical Bath Deposition (CBD) technique is found most promising for achieving high-efficiency solar cell. In the present study, we have deposited CdS thin films on soda-lime glass by two different methods (a) thermal evaporation and (b) CBD. In the CBD method, conformal coverage of the compound takes place.

5.2 Experimental Details

CdS thin films were deposited by three different techniques, (a) thermal deposition, (b) Chemical Bath Deposition (CBD), and (C) Radio Frequency (RF) Sputtering on a 60 x 60 x 1mm SLG substrate. CdS thin films deposited

by thermal evaporation at different substrate temperature (ST) [Room Temperature (RT), 100, 125, 150 and 175 °C] with a thickness of 50 nm. Pure CdS powder from SIGMA-ALDRICH (99.995 %), USA has been used for thermal deposition. The source to substrate distance was maintained at 8 cm. The substrate temperature was measured by chromel - alummel thermocouple using a temperature controller. The rate of deposition and thickness of thin films deposited by thermal evaporation was estimated by thickness monitor Hind High Vacuum Co. India (HHV DTM-110). Cadmium sulphate ($CdSO_4$), ammonia, thiourea ($SC(NH_2)_2$) were used as an initial precursor for depositing CdS by CBD technique. CdS deposited by chemical bath deposition (CBD) with different S/Cd ratio i. e., [1 (sol 1), 2.5 (sol 2), 5 (sol 3), 7.5 (sol 4)]. The cadmium (0.02 M) concentration was kept constant while sulphur concentration was varied i. e. (0.2, 0.5, 1, 1.5 M) and the pH of the bath was maintained to 10.6. The glass substrate was rotated vertically in the bath. The solution was continuously stirred to deposit homogenous CdS thin film. The total volume of solution was 700 ml and bath temperature was maintained 65-67 °C. 2-inch (diameter) CdS was used to deposit CdS thin film using RF-sputtering. The working was 3.5 mTorr, 30 W RF power, and substrate temperature was maintained to 300 °C. Thickness was 80 nm and substrate was rotated for uniformity.

5.3 Results and Discussion

5.3.1 Structural Characterization

Structural characterization of CdS thin films deposited by (a) thermal evaporation at different substrate temperatures, (b) CBD with different S/Cd ratios, and (c) RF-sputtered have been determined from X-ray analysis. X-ray analysis of CdS thin films deposited by all three deposition techniques are shown in Fig. 5.2 (a), (b), and (c). CdS exhibit two phases i.e. (a) hexagonal and (b) cubic. The preferable phase of CdS for n-type buffer layer to form a p-n junction with p-type CIGS is hexagonal. This is because CIGS possesses a tetragonal phase structure, so to avoid lattice mismatch hexagonal phase is

Fig. 5.1: Chemical Bath Deposition process for CdS thin film deposition.

preferred rather than cubic. The major peak at 26.7 was observed for CdS thin films which refer to the prime hexagonal phase (*002*) [14, 15]. At ST 150 °C, the intensity of peak is highest which shows the homogeneous deposition of a thin film with stoichiometric composition. No other phase had been found in CdS S/Cd ratio thin films deposited by thermal evaporation. XRD analysis of CdS thin films deposited by CBD technique reflects the presence of another phase (110) also [16, 17]. The hexagonal phase has been confirmed with JCPDS card 41-1049, a-CdS phase. More enhanced crystallography of the CdS layer was observed when deposited using the RF-sputtering technique [18]. Not only (*002*) and (*110*) phases but (*201*) was also observed as shown in Fig. 5.2 (c).

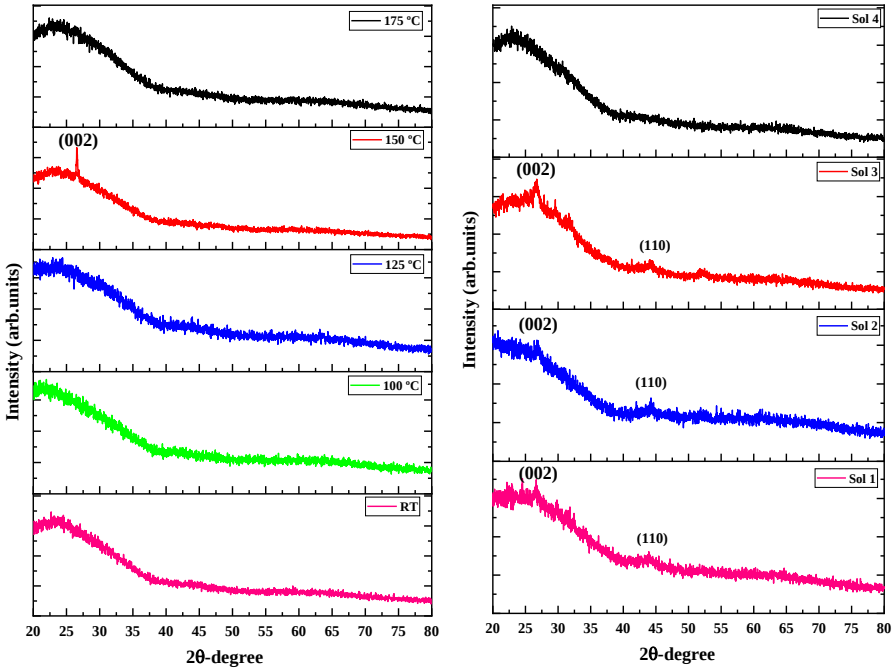

(a) **(b)**

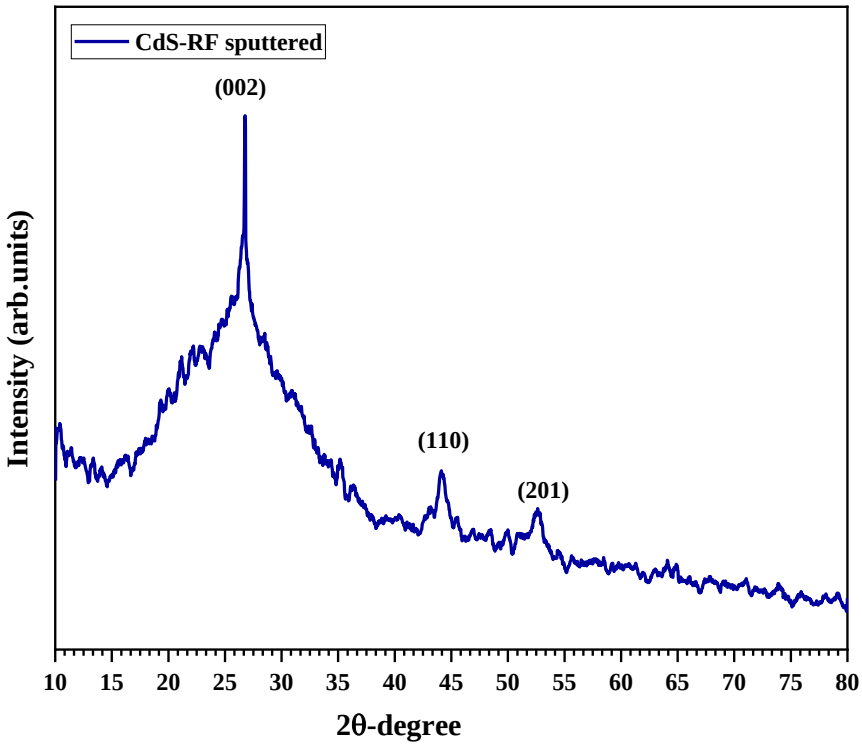

(c)

Fig. 5.2: X-ray analysis of CdS thin films deposited by (a) thermal evaporation at different ST, (b) CBD at different S/Cd ratio, and (c) RF sputtered.

5.3.2 Optical Analysis

Optical Characterization is one of the key parameters to analyse the quality of deposited thin films. The transmittance of all CdS thin films deposited by (a) thermal at different ST, (b) CBD at different S/Cd ratio, and (c) RF sputtered has been measured as shown in Fig. 5.3 (a), (b), and (c). The average transmittance of CdS thin films deposited at substrate temperature is nearly 75-90 % while those films deposited by CBD have a transmittance of 52-74 %. The transmission of CdS thin film deposited by thermal evaporation at substrate temperature RT, 100, 125, and 175 °C decreases with increment in wavelength. This may be due to the inhomogeneous deposition of CdS thin film. It is also a well-known fact that Cd^{+2} adheres faster than S^{-2} ions, due to which many defects like vacancies, interstitials, dislocation, strain have been formed during deposition. Due to high vapor pressure and low adhesion of sulphur atoms, the stoichiometric composition is not maintained at RT, 125, and 175 °C ST. CdS thin film with an S/Cd ratio of 1 and 7.5 has a high transmission. This is due to the ion-by-ion growth mechanism which leads to crystal growth. Low transmission in S/Cd ratio 2.5 and 5 is due to colloidal agglomeration cluster formation in the solution. Colloidal aggregates form due to the ammonia complex. CdS thin film with S/Cd ratio of 7.5 has the highest transmission due to less defect density and uniform coverage of the film. Similarly, the film deposited at 150 °C ST has homogenous deposition with uniformity has high transmission. Similarly, the RF-sputtered CdS layer has transmittance above 90 %. As shown in Fig. 5.3 (c). The band gap has been estimated from (absorption coefficient x thickness) vs energy plot is shown inset Fig. 5.3 (a), (b), and (c). The bandgap of CdS thin films deposited by thermal evaporation is nearly in the range of 2.25-2.34 eV which is in good agreement with bulk CdS (2.42 eV). At 150 °C, the substrate temperature band gap is nearly 2.34 eV which is due good crystallinity of the deposited thin films [19]. For CdS, thin films deposited by CBD have a bandgap of nearly 2.25 eV with an S/Cd ratio of 7.5. This indicated higher S/Cd ratio has good crystallinity compared to a lower S/Cd ratio. It has been noticed that at a higher S/Cd ratio conformal coverage CdS

over the glass substrate is good. While for the RF-sputtered CdS layer, the bandgap of 2.32 eV was recorded. The blue shift in bandgap energy of CdS thin films from the bulk CdS (2.42 eV) is due to the formation of defects. These defects are the traps that affect optical absorption. The decrease in the optical bandgap is due to defect-induced band tailing. Band tailing below the absorption edge is due to the formation of the location of localized energy states near band edges. It has also been reported that a decrease in optical bandgap is due to confinement of charge carrier [20-21].

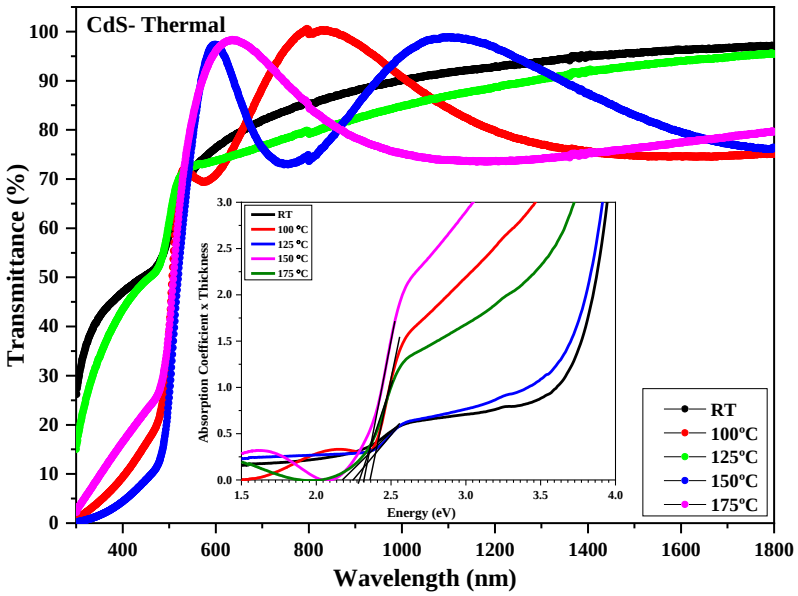

(a)

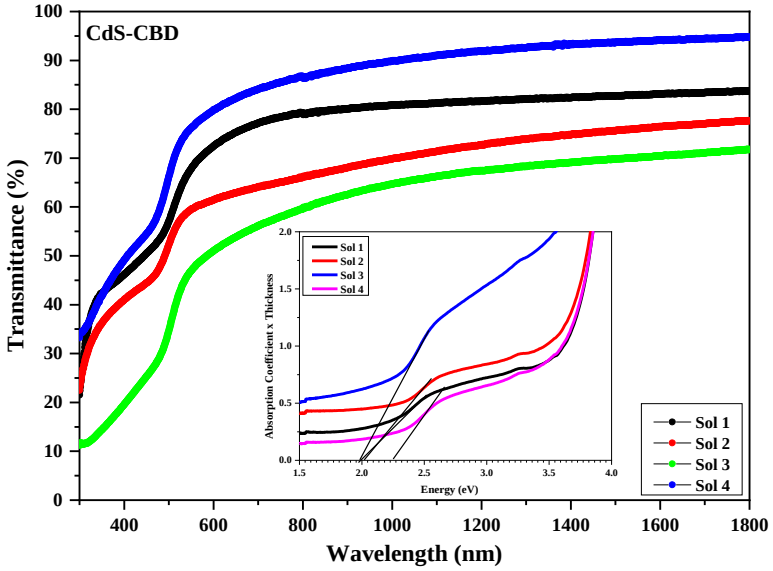

(b)

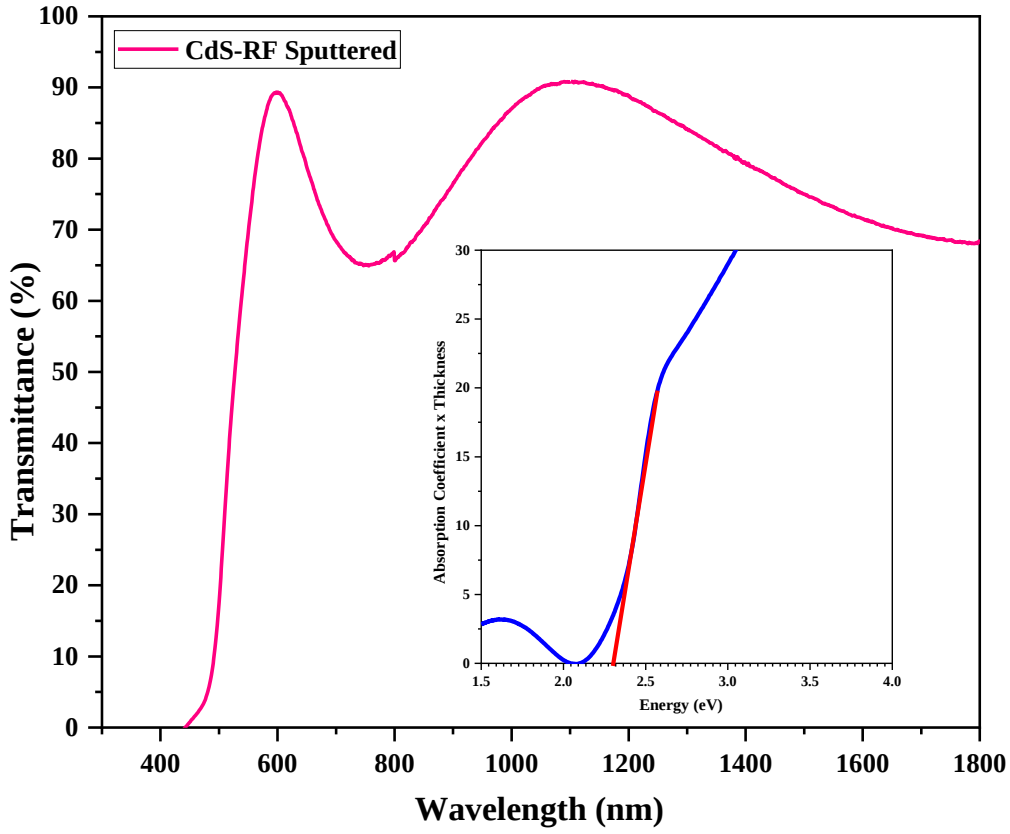

(c)

Fig. 5.3: Optical Transmittance spectra and Optical Bandgap (inset) of CdS thin films deposited by (a) thermal evaporation at different ST, (b) CBD at different S/Cd ratio, and (c) RF sputtered.

5.3.3 Electrical Characterization

Urbach energy is also known as “band tail width” as-sociated with localized states of amorphous structure in forbidden gap. Urbach energy is governed by the structural disorder, an imperfection in stoichiometric and passivation at the surface [22]. Urbach energy also indicates the dis-order of phonon states in the film. Urbach energy ‘E_U’ is found below the absorption band edge of the compound. The generation of absorption edge at the bandgap energy is due to exciton–phonon interaction or may be due to electron-phonon interaction. This can be estimated from the steepness parameter. The band bending causes a reduction in the optical bandgap. The higher E_U defines the high disorder of

phonon states in the films. The high disorder of phonon states in CdS thin films may be due to thermal disorder or occupancy level of phonon states. The Urbach energy (E_U) and steepness parameter (σ) has been estimated for CdS thin film deposited by thermal evaporation and CBD as a function of ST and S/ Cd ratios and RF sputtered is shown in table 5.1. It has been found that CdS thin film deposited at ST 150 °C has E_U = 34.34 meV, while that with S/Cd ratio 5 has E_U = 54.46 meV. The results indicate that, at RT, 100, 125, and 175 °C substrate temperature, a high disorder in the film is present due to improper stoichiometric composition [23]. For CdS thin films deposited at different S/Cd ratios, at a higher S/Cd ratio the disorder decrease, due to uniform deposition of CdS. Some studies are based on the correlation between Urbach energy open circuit voltage, short circuit current, and quantum efficiency [24, 25]. The electrical resistivity of CdS thin-films also had been measured and mention in Table 5.1. It has been noticed the change in electrical resistivity of CdS thin film in light and dark conditions i.e., the photoconductive response of CdS thin-films. The electrical resistivity is in order of 10^5 Ω-cm [26].

Table 5.1: Urbach Energy, Steepness parameter, Light and Dark Resistivity of CdS thin-film.

As grown sample		**Urbach Energy (E_U meV)**	**Steepness parameter (s)**	**Light Resistivity (10^5 Ω-cm)**	**Dark Resistivity (10^5 Ω-cm)**
At different substrate temperature (°C)	RT	73.52	6.86	6.86	6.05
	100	43.76	6.12	6.12	8.64
	125	70.52	6.31	6.31	12.05
	150	34.44	5.31	5.31	18.34
	175	55.34	5.56	5.56	15.52
At different S/Cd ratio	Sol 1	82.98	2.72	2.72	5.98
	Sol 2	82.03	3.41	3.41	5.08
	Sol 3	54.46	4.46	4.46	6.42
	Sol 4	78.74	2.03	2.03	7.18
RF-Sputter	30 W, 3.5 mTorr	47.38	3.93	1.6	3.81

5.3.4 Photoluminescence Analysis

To study the defect formation photoluminescence analysis has been carried out. Pl scrutinizes optically active recombination centers. Photoluminescence

analysis provides information regarding impurities and defect centers which act as recombination centers for charge carriers that are responsible for the degradation of efficiency of the solar cell. In CdS material photocurrent is not generated due to radiative or non-radiative recombination, because it contains highly compensated with comparable densities of shallow donors and deep acceptors. Pl analysis of CdS thin films deposited by thermal evaporation, CBD, and RF-sputtered techniques has been studied. An emission peak around 1.74 eV has been found in all deposited CdS thin films. Fig. 5.4 (a), (b), and (c) shows the Pl analysis of CdS thin films deposited by thermal evaporation, CBD, and RF-sputtering technique. The peak at energy 1.74 eV is known as the 'Red band'. Red band' with energy 1.74 eV is due to sulfur vacancies. Pl intensity of CdS thin films decreases as substrate temperature increase from RT to 150 °C. This indicates that as the substrate temperature increases the defect density decreases. But at higher substrate temperature i. e., 175 °C, Pl intensity increased. This increase in Pl intensity is due to an increase in defect density [27, 28]. Pl intensity of CdS thin film deposited by CBD technique decreased with the increase in S/Cd ratio. As the concentration of sulfur atoms increase, the defect density of sulfur defect decrease. The Pl spectra of CdS thin films deposited by thermal evaporation and CBD technique have a gaussian shape which is due to the photophysical result of the band measurement of the thin film at room temperature. The broadening of shape is due to the in-homogenous distribution of cadmium and sulfur atoms and the thermal energy associated with it. The Pl emission is not sharpened because of the presence of recombination sites, different impurity concentration is present in grains. It is also noted that the red band of CdS thin films is generated due to the transition of electrons trapped in surface states to the valence band. This type of transition occurs in the formation of crystallographic defects [29].

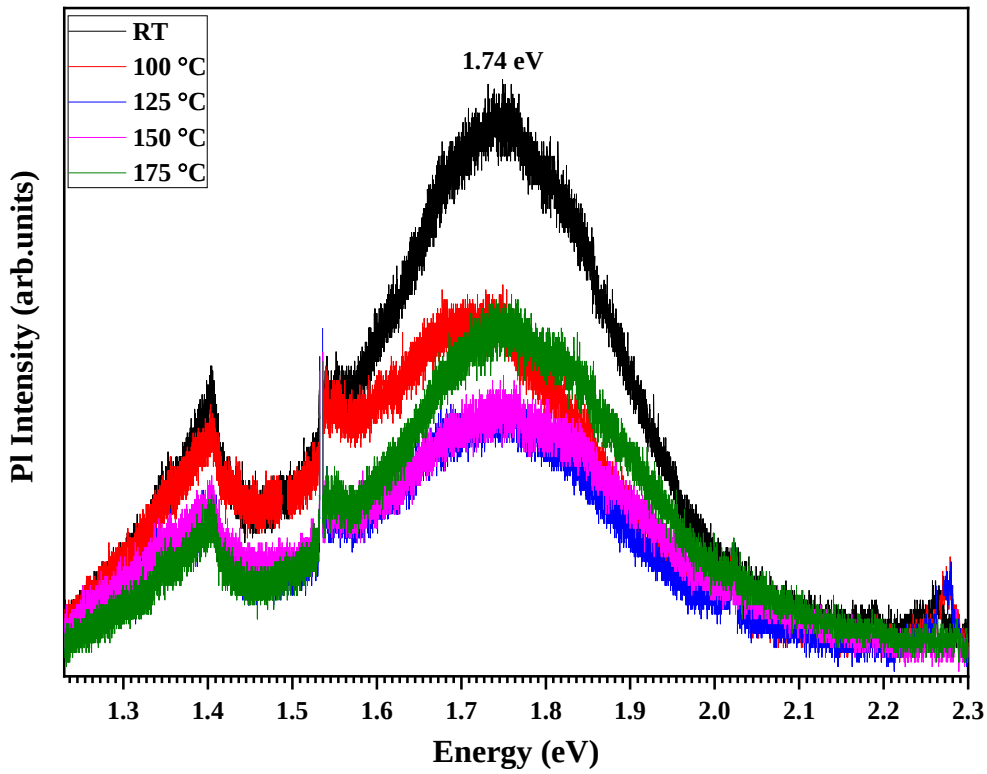
RT
100 °C
125 °C
150 °C
175 °C
1.74 eV
Pl Intensity (arb.units)
1.3
1.4
1.5
1.6
1.7
1.8
1.9
2.0
2.1
2.2
2.3
Energy (eV)

(a)

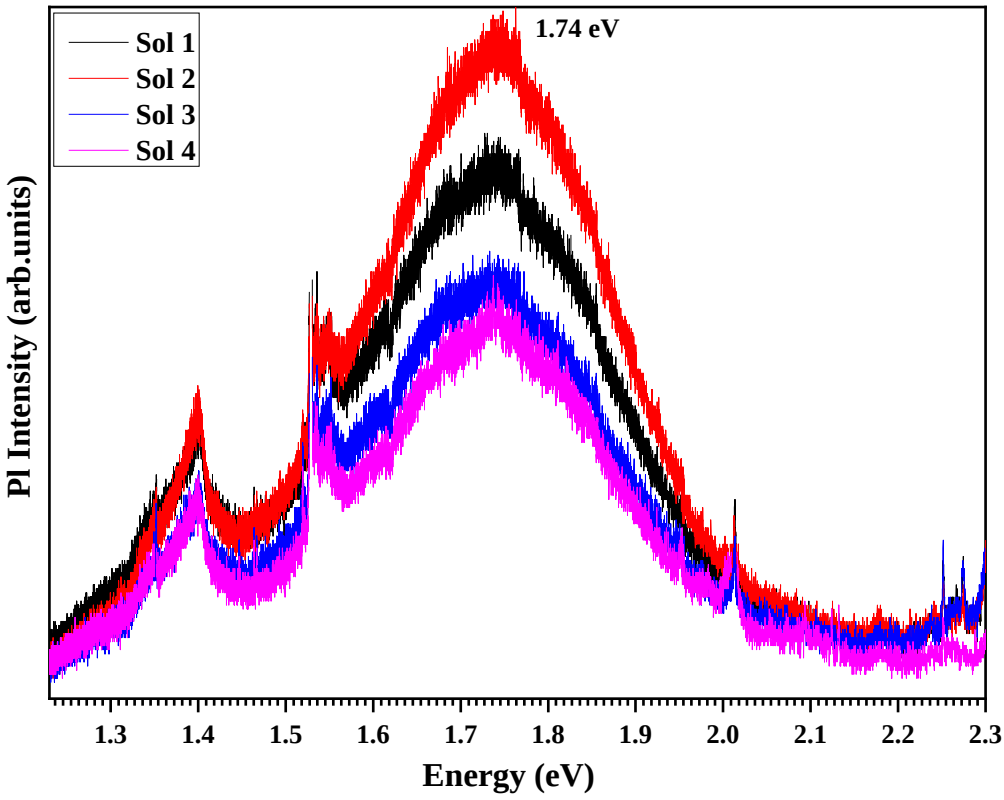
Sol 1
Sol 2
Sol 3
Sol 4
1.74 eV
Pl Intensity (arb.units)
1.3
1.4
1.5
1.6
1.7
1.8
1.9
2.0
2.1
2.2
2.3
Energy (eV)

(b)

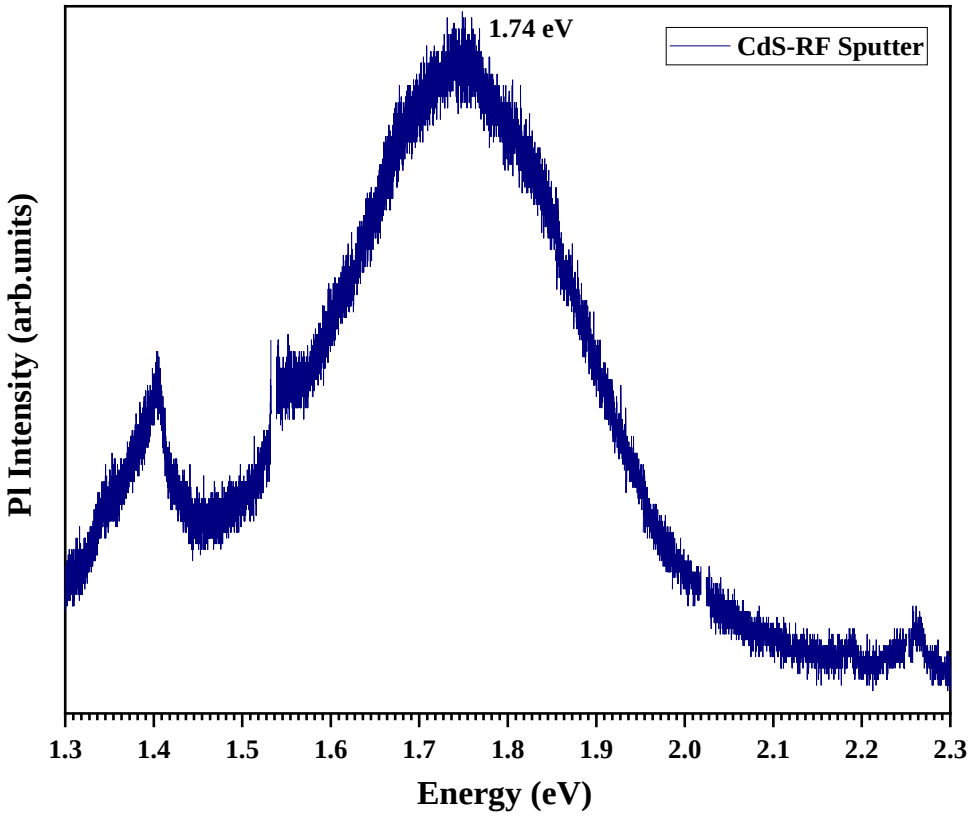

(c)

Fig. 5.4: Photoluminescence spectra of CdS thin films deposited by (a) thermal evaporation at different ST, (b) CBD at different S/Cd ratio, and (c) RF sputtered.

5.3.5 Scanning Electron Microscopic Analysis

As a protective barrier layer, n-CdS thin-film should possess a uniform conformal coverage without pinholes to reduce the short circuit path between the top window and absorber layer. Microstructural analysis of the CdS layer deposited by all three deposition techniques shown in Fig. 5.5 has been examined. At substrate temperature 150 °C, pinholes or pits were observed as shown in Fig. 5.5 (a). Well here growth is channeled, this may be due to vapor pressure and condensation difference of cadmium and sulfur ions at the substrate surface. Well uniform coverage as shown in Fig. 5.5 (b) was noticed for CdS thin-film deposited by CBD technique. Ion-by-Ion growth mechanism produces a smooth, dense, and uniform surface without pinholes, pits, or dent.

RF-sputtered CdS thin-film possesses a mildly rough surface [30]. The grains are uniformly distributed over the surface, but few grains are agglomerated to form approximate spherical grains comparatively bigger in size as shown in Fig. 5.5 (c). As such here also no pinholes were observed.

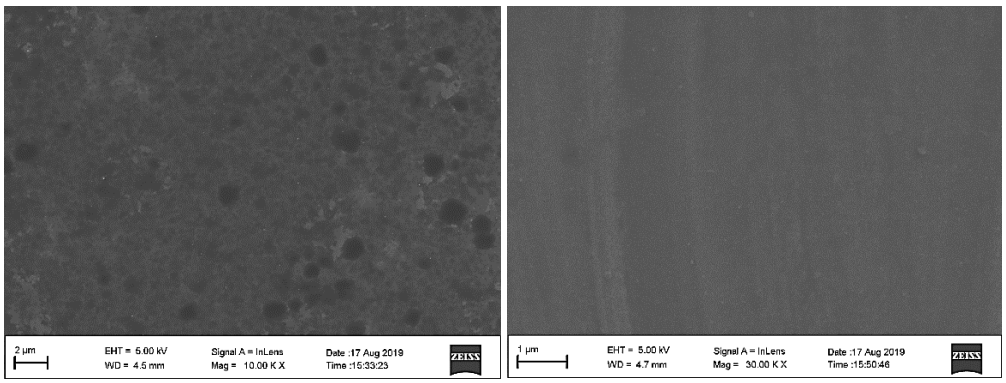

(a) **(b)**

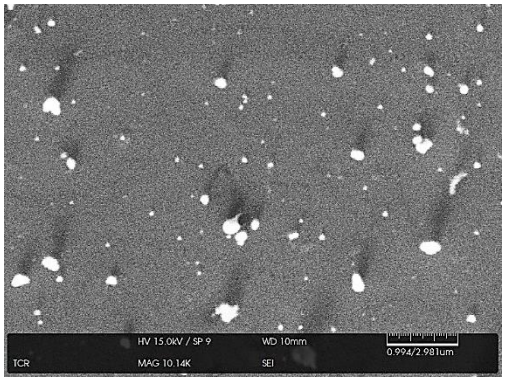

(c)

Fig. 5.5: Scanning Electron Microscopic images of CdS thin films deposited by (a) thermal evaporation ST-150 °C, (b) CBD at different S/Cd ratio, and (c) RF sputtered.

CdS layer was deposited by chemical bath deposition technique at different duration. The role of the buffer layer is not only to form the n-type junction with the absorber layer also to reduce the short circuit due to pinholes. It also passivates the absorber and protects it from getting damaged by highly energetic RF-sputtered AZO ions. CdS layer with a duration of 3 min, 6 mins, 7 mins, 8 mins, 9 mins, and 10 mins were deposited Fig. 5.6 represent the photographic image of the CdS layer with different duration.

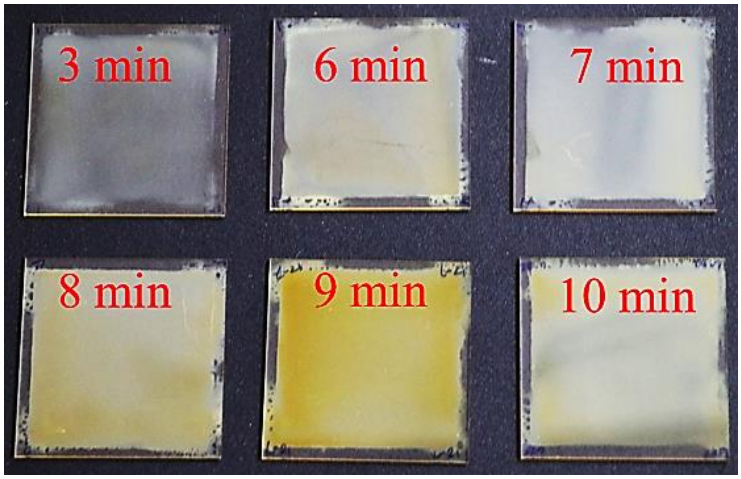

Fig. 5.6: Photographic image of CdS layer deposited by CBD technique at the different duration of deposition.

CdS layer deposited for 8 mins have better conformal coverage without pinholes. The elemental dispersive x-ray analysis of the CdS layer deposited for 8 mins has been analyzed as shown in Fig. 5.7 which confirms the elemental composition of the CdS layer. thus, the CdS layer deposited for min is suitable as a buffer layer for developing CIGS solar cell module.

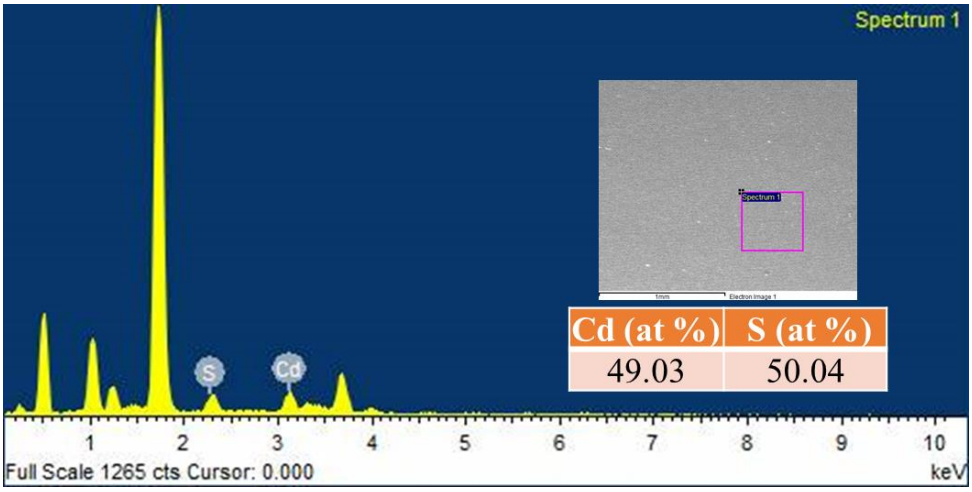

Fig. 5.7: Elemental dispersive x-ray analysis of CdS layer deposited by CBD technique for 8 mins.

5.3 P2 Patterning: Laser and Mechanical Scribing

The laser scribing process is a widely accepted approach for the fabrication of highly efficient module. After P1 isolation on the Mo layer, the absorber (CIGS)

and buffer (CdS) has been deposited. To make cell interconnection, both CIGS and CdS layer has to 'ablate or scribe' creating a series connection with adjacent cell. This helps to reduce the ohmic loss between front and back contact. Ultrafast Picosecond and Femtosecond laser are used for selective ablation of CIGS and CdS layer. Here the layer has been ablated by the 'Lift-off' process where the Mo layer remains undamaged.

For the fabrication of the 50 x 50 mm CIGS solar cell module, an attempt of P2 scribe with nanosecond 532 nm laser was carried out. Fig. 5.8 demonstrates P2 scribing evaluation. The Pulse repetition rate is 20 kHz, scribing speed 40 mm/sec, 2-pass has processed while the pulse energy 1.5 µJ, 2.1 µJ, and 2.4 µJ for P2 shown in Fig. 5.8 (a), (b), and (c). For low pulse energy P2 has not completely ablated. Melts and debris are still observed shown in Fig. 5.8 (a) which confirms the presence of elements of absorber and buffer layer. increasing pulse energy to 2.1 µJ trench has been observed in the central middle regime only and at the edges melts have been accumulated. Further on increasing pulse energy to 2.4 µJ, clean ablation without heat-affected zone at edges was observed. Mechanical scribing of P2 was also carried out by fine needle shown in Fig. 5.8 (d).

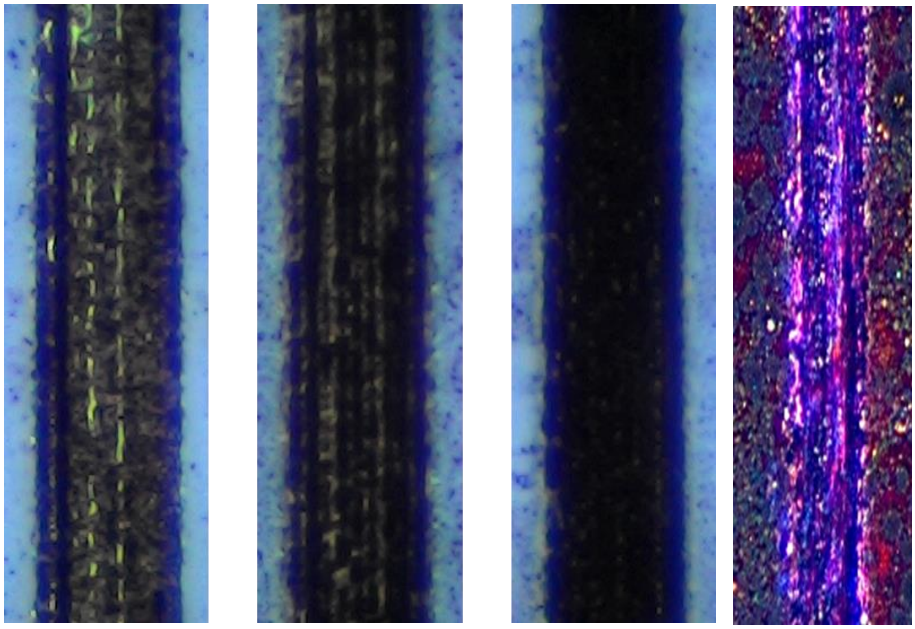

(a) **(b)** **(c)** **(d)**

Fig. 5.8: P2 scribe using 532 nm laser, pulse repetition rate 20 kHz, 40 mm/sec scribing speed and pulse energy (a) 1.5 µJ, (b) 2.1 µJ, and (c) 2.4 µJ and (d) P2 mechanically scribed.

Conclusions

Cadmium Sulphide layer as buffer layer in the fabrication of the CIGS solar cell module is studied here. CdS thin-film was deposited by thermal-evaporation at different substrate temperatures, chemical bath deposition (CBD) with different S/Cd ratios, and RF-sputtering technique. Physical, microstructural, optical, Urbach energy, electrical resistivity, and photoluminescence properties were analyzed. From the analysis, it was found that CdS layer deposited by CBD is suitable as a buffer layer for CIGS solar cells. Further, CdS layer at different duration was deposited and it was found that for 8 min of deposition duration, conformal coverage was observed. P2 mechanical patterning was carried out by both 532 nm laser and mechanical scribing techniques.

References

[1] M. Nakamura, K. Yamaguchi, Y. Kimoto, Y. Yasaki, T. Kato and H. Sugimoto, *IEEE Journal of Photovoltaics*, **9 (6)** (2019) 1863-1867. Philip Jackson, Dimitrios Harriskos, Roland Wuerz, Oli- ver Kiowski, Andreas Bauer, T. F. Magorian, and Michael Powalla, *phys. status solidi RRL* **9 (1)** (2015) 28 1-4.

[2] H. Moualkia, S. Hariech, and M. S. Aida, *Thin Solid Films* **518**, (2009) 1259-1262.

[3] Seok Hwan Yoon, Seung Soo Lee, Kook Won Seo, and Il-Wun Shim, *Bull. Korean Chem. Soc.* **27** (12) (2006) 2071-2073.

[4] A. I. Oliva, R. Castro-Rodríguez, O. Solís-Canto, Víctor Sosa, P Quintana, and J. L. Peña, *Applied Surface Science*, **205 (1-4)** (2003) 56-64.

[5] F. Lisco, P. M. Kaminski, A. Abbas, K. Bass, J. W. Bowers, G. Claudio, M. Losurdo, J. M. Walls, *Thin Solid Films*, **582** (2015) 323-327.

[6] Krishnaiah Mokurala, Lauryn L. Baranowski, Francisco W. de Souza

Lucas, Sebastian Siol, Maikel F. A. M van Hest, Sudhanshu Mallick, Parag Bhargava, and Andriy Zakutayev, *ACS Comb. Sci.,* **18** (2016) 583-589.

[7] Jeng-Shin Ma, Subrata Das and Chung-Hsin Lu, *RSC Adv.***, 6** (2016)107886-107893.

[8] Marwa Fathy, Abd El-Hady B. Kashyout, Shaimaa Elyamny, Gamal D. Roston, Ahmed A. Bishara, *Int. J. Electrochem. Sci.,* **9** (2014) 6155-6165.

[9] Ji Hyun Choi, Sung Hee Jung & Chee Won Chung, *Journal of the Korean Physical Society,* **68** (2016) 425-430.

[10] Mikel Sanz, Rebeca de Nalda, Jose F. Marco, Jesus G. Izquierdo, Luis Bañares, and Marta Castillejo, *J. Phys. Chem. C*, **114** (2010) 4864-4868.

[11] Violeta Popescu and Horea Iustin Na'cu, *Chalcogenide Letters* **3 (9)** (2006) 67-72.

[12] V. P. Kladko, O. S. Lytvyn, P. M. Lytvyn, N. M. Osipenok, G. S. Pekar, I.V. Prokopenko, A. F. Singaevsky, and A. A. Korchevoy, *Semiconductor Physics, Quantum Electronics & Optoelectronics,* **5 (2)** (2002) 170-175.

[13] Y. Sánchez, M. Espíndola-Rodríguez, H. Xie, S. López-Marino, M. Neuschitzer, S. Giraldo, M. Dimitrievska, M. Placidi, V. Izquierdo-Roca, F.A. Pulgarín-Agudelo, O. Vigil-Galán, and E. Saucedo, *Solar Energy Materials and Solar Cells*, **158 (2)** (2016) 138-146.

[14] N. M. Shah, J. R. Ray, M. S. Desai, and C. J. Panchal, *Journal Of Optoelectronics And Advanced Materials*, **12 (10)**, (2010), 2052-2056.

[15] L. Huang, Z. L. Wei, F. M. Zhang, and X. S. Wu, *Journal of Alloys and Compounds*, **648** (2015) 591-594.

[16] Salah Abdul-Jabbar Jassim, Abubaker A. Rashid Ali Zumaila, and Gassan Abdella Ali Al Waly, *Results in Physics*, **3** (2013) 173-178.

[17] W. G. C. Kumarage, L. B. D. R. P. Wijesundara, V.A. Seneviratne, C. P. Jayalath, and B. S. Dassanayake, *Procedia Engineering* **139** (2016) 64-68.

[18] N. K. Das, J. Chakrabartty, S. F. U. Farhad, A.K. Sen Gupta, E. M. K. Ikball Ahamed, K. S. Rahman, A. Wafi, A. A. Alkahtani, M.A. Matin, and N. Amin, Results in Physics **17** (2020) 103132 (1-8)

[19] Baljinder Singh, Janpreet Singh, Jagdish Kaur, R.K. Moudgil, and S.K.

Tripathi, *Physica B: Condensed Matter* **490** (2016) 49-56.

[20] L. Huang, Z.L. Wei, F.M. Zhang, X.S. Wu, *Journal of Alloys and Compounds*, **648** (2016) 591-594.

[21] Andre Slonopas, Herbert Ryan, Benjamin Foley, Zeming Sun, Keye Sun, Tatiana Globus, and Pamela Norris, *Materials Science in Semiconductor Processing*, **52** (2016) 24-31.

[22] Ihor Studenyak, Mladen Kranjec, and Mykhailo Kurik, *International Journal of Optics and Applications*, **4(3)** (2014) 76-83.

[23] M.A. Islam, M.S. Hossain, M.M. Aliyu, P. Chelvanathan, Q. Huda, M.R. Karim, and K. Sopian, N. Amin**,** *Energy Procedia*, **33** (2013) 203-213**.**

[24] M. Solomon, A. Johnson, Elements: Boston College Under- graduate *Res. J*., **11 (1) (**(2015) 7896 (1-4).

[25] M. Troviano, K. Taretto, *EU PVSEC Proceedings of 24th Eu- ropean Photovoltaic Solar Energy Conference 21-25 September 2009, Hamburg, Germany*, **2933** (2009) 2933-2937.

[26] Sung-Gi Hur, Eui-Tae Kim, Ji-Hong Lee, Geun-Hong Kim, and Soon-Gil Yoon, *J. Vac. Sci. Technol. B*, **26 (4)** (2008) 1334-1337.

[27] Frédérique Gemain, Ivan-Christophe Robin, Sébastien Renet, and Sergio Bernardi, *Phys. Status Solidi C*, **9 (8-9)** (2012) 1-4.

[28] Rajeev R. Prabhu and M. Abdul Khadar, *Bull. Mater. Sci.*, **31 (3)** 2008 511-515.

[29] J Aguilar-Hernandez ´, G Contreras-Puente, A Morales-Acevedo, O Vigil-Galan´, F Cruz-Gandarilla, J Vidal-Larramendi, A. Escamilla-Esquivel, H. Hernandez-Contreras´, M Hesiquio-Garduno˜, A. Arias-Carbajal, M Chavarr´ıa-Castaneda ˜ and G. Arriaga-Mej´ıa, *Semicond. Sci. Technol*, **18** (2003) 111-114.

[30] Linquan Zhang, Jinchun Jiang, Wei Wang, Xiaoxu Huang, Qi Yuan, Ruijiang Hong, and Limei Cha, *Journal of Materials Science: Materials in Electronics*, **29** (2018) 29 7637-7643.